

# Computational Topology for Reconstruction of Surfaces with Boundary: Integrating Experiments and Theory

K. Abe

Department of Mathematics  
University of Connecticut  
Storrs, CT 06269 USA  
abe@math.uconn.edu

T. J. Peters

Department of Computer Science  
Department of Mathematics  
University of Connecticut  
Storrs, CT 06269 USA  
tpeters@cse.uconn.edu

D. R. Ferguson

DRF Associates  
Seattle, WA  
DRF.ASSOC@comcast.net

J. Bisceglia

Department of Computer Science  
University of Connecticut  
Storrs, CT 06269-3155 USA

A. C. Russell

Department of Computer Science  
Department of Mathematics  
University of Connecticut  
Storrs, CT 06269 USA  
acr@cse.uconn.edu

Takis Sakkalis

Agricultural University of Athens  
Athens, 118 55 Greece, and  
Massachusetts Institute of Technology  
Cambridge, MA 02139, USA  
stp@aua.gr

## Abstract

*In order for surface reconstruction to comprehensively include surfaces with boundary as a complement to existing approaches for surfaces without boundary, we report new techniques and theory in computational topology. Our approach is motivated from differential geometry and differential topology. We have also conducted significant experimental work to test our resultant implementations. We elucidate some subtle issues that can arise regarding the roles of the medial axis and sampling density. The crucial topics for  $C^2$  manifolds are*

- 1. important defining properties of  $C^2$  manifolds with boundary,*
- 2. approximation of normals, particularly along the boundary,*
- 3. sampling density, and*
- 4. successful practical algorithms and examples.*

**Keywords:** surface reconstruction, twice-differentiable

**manifold, differential topology, differential geometry, medial axis.**

## 1. Introduction and Motivation

The primary contribution of this paper is to present new theory and techniques for topology-preserving reconstruction and approximation of surfaces. This paper reports on mature results regarding

1. computational topology properties of  $C^2$  manifolds with boundary, and
2. successful practical algorithms and examples.

Partial results are reported, regarding

1. approximation of normals, particularly along the boundary and
2. sampling density.

For each surface  $M$  with boundary, we construct an auxiliary surface, called its *envelope*. We use the envelope to perform approximation and reconstruction of surfaces, inclusive of those with or without boundary. We discuss our implementation of code that enriches the class of surfaces that can be considered, and we articulate the supporting practical algorithms that are derived from our theoretical and experimental investigations.

A comparison between the images of Figure 1 and Figure 2 show the value of our method. An original trefoil surface was created for these experiments by a linear extrusion of a trefoil curve, so as to produce no self-intersections. This trefoil surface is like a ribbon with the corresponding knot for its two boundary curves. Figure 1 is a series of reconstructions using the envelope technique with different sample densities, with the density decreasing from left to right. Figure 2 is the same using direct reconstruction from the PowerCrust algorithm. We note that, for the same sampling densities, the method based upon use of the envelopes in Figure 1 appears to converge nicely to the desired trefoil surface, while the direct reconstruction of Figure 2 does not. We note that the Power Crust algorithm was not designed to accept surfaces with boundary. However, in practice, the Power Crust has been found to be useful for reconstruction of some surfaces with boundary, with possible reliance upon *ad hoc* modifications [6]. Hence, our interest in our comparisons is to begin to formalize a rich admissible class of input surfaces for a provable implementation of ambient isotopic approximations. A related example is presented for an unknot surface in Section 6.2.

Several recent approaches to topology-preserving surface approximation have been restricted to  $C^2$  2-manifolds without boundary [5, 7, 9, 15, 24]. For some practical surface reconstructions, a heuristic method has proven generally successful for approximation of some manifolds with boundary [6]. In a related article [15] on surface reconstruction for computer-aided geometric design, questions were posed about the possibility of creating algorithms for surfaces with boundary. The approach offered here is responsive, postulating new assumptions for input to be sufficient for approximation of surfaces with boundary. While some methods [3, 4, 11] have had some success reconstructing surfaces with boundary, the scope of the class of admissible surfaces with boundary was not definitively articulated and was presented as a result of experimental observation. This work specifically provides new theory that all  $C^2$  surfaces with boundary can have arbitrarily close ambient isotopic reconstructions (dependant, of course, upon sufficient sampling density, corroborating other published results [11]) and shows resultant practical implementations.

As initial motivation for the practical value of our results, we refer to Figure 3, below. The object to be reconstructed is a cylinder with boundary curves at both ends,

having no top or bottom. The left side of Figure 3 is representative of the results that could be expected from many contemporary algorithms whereas the right side of Figure 3 shows our significantly improved output.

The paper is organized as follows: In Section 2, we summarize related work. Section 3 provides an overview of the theory and extensions. Implementation and graphical experiments of these new techniques are presented in Section 4. Section 5 contains a discussion of hypotheses about admissible input data for our techniques. Section 6 presents observations about the influence of normal approximations and sampling densities. Closing remarks are given in Section 7.

## 2. Related Work

An emphasis upon topological guarantees for surface approximants has recently appeared in the literature on surface reconstruction [5, 7, 9, 15]. For surface reconstruction, it is typical that only point cloud data is assumed to be available, while the methods presented here rely formally on maximal curvature and minimal separation distances. For our foot example, which is based upon point cloud data, we estimated these geometric values in order to perform an improved surface reconstruction. These curvature and separation values will often be available for reverse engineering of manufactured objects [20]. While our reliance upon these values remains the subject of further study, the methods presented here will be directly applicable in many graphics applications, when the surface definitions will already be given and the relevant problem will be to produce a topologically correct approximation. For instance, related earlier work by some of the present authors [10] has been used to prevent undesirable topological changes during object deformations [17] for animations. The methods presented here will provide even more general criteria for an animator to preserve the critical topological characteristics of an object as it changes across successive frames. Some previous topological guarantees relied upon knowledge of the medial axis [3, 4, 5, 7, 13, 15, 16], which implicitly captures this curvature and separation information. We continue to look for unifying themes, but it should be clear that some estimation of a bound on surface curvature is crucial to any well-defined surface approximation method.

The theoretical concerns in providing topological guarantees for surface approximations near boundaries have been presented in the literature [6, 15, 18] within the context of approximants created during surface reconstruction. In particular, the paper [6] presents a heuristic argument to reconstruct a surface with boundary, with a relevant example being the reconstruction of a foot. In a different approach [15], a similar example of a foot is reconstructed as a manifold with boundary to avoid undersampling prob-

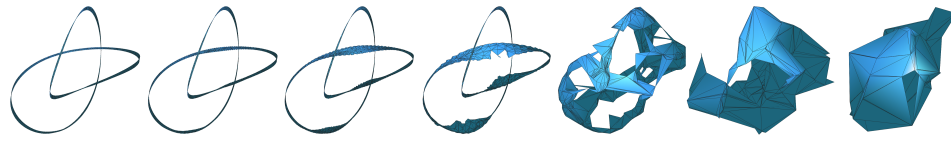


**Figure 1. Trefoil A**

---

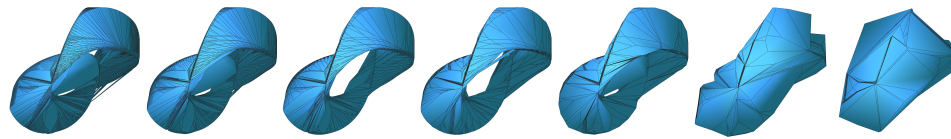


**Figure 2. Trefoil B**

---

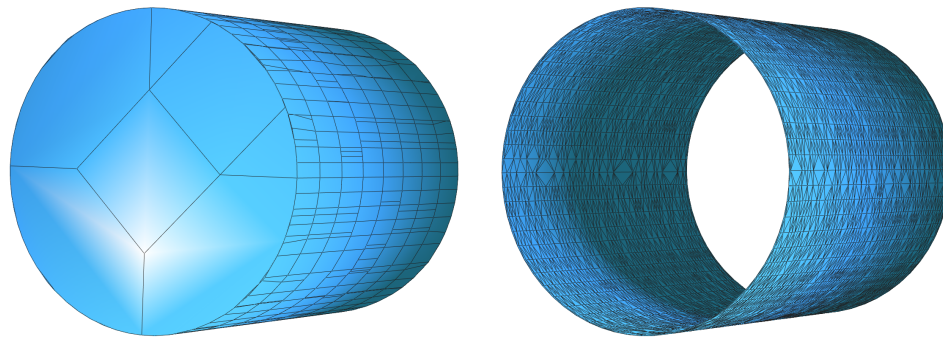


**Figure 3. Comparison of Methods for Cylinder**

---

lems often experienced near the boundary. Both of these approaches for boundaries [6, 15] were pragmatic responses to the known difficulties of reconstruction of boundaries from unorganized sample points. As these approaches depend upon an approximation of the medial axis, it is worth noting that it has since been shown [18] that the typical sampling input for surface reconstruction is not sufficient, in general, to permit a topologically faithful reconstruction of the medial axis of the surface with boundary.

The value in preferring ambient isotopy for topological equivalence versus the more traditional equivalence by homeomorphism [26] has previously been presented [9, 24] and the interested reader is referred to those papers or to a standard mathematical text [19] for formal definitions. Intuitively, two closed curves will not be ambient isotopic if they form different knots, which can only be converted into each other by “untying” one knot and retying it to conform to the other, even while all knots are homeomorphic. For curves, a theorem has been published that provides for ambient isotopic piecewise linear (PL) approximations of a specifically described class of curves [21], inclusive of both those with and without boundary points, motivating the present investigation to surfaces with boundary. Our methodology uses the concept of the envelope of a surface, which has previously been presented in the context of tool-path generation for a specialized class of parametric surfaces [23].

The present work emphasizes the integration of concepts from low-dimensional topology and differential geometry into the emerging sub-discipline of computational topology, as a complementary contribution to the incorporation of combinatorial topology and computational geometry formalisms that have already appeared [8, 14, 22].

### 3. Preliminaries and Theory

In order to keep this section short, we refer the reader to standard definitions of a manifold with boundary [12], which are also summarized by the present authors in technical reports available on-line [1, 2]. As an intuitive overview, it suffices to observe that the differentiable properties along the boundary must follow as continuous limits of the corresponding differentiable properties within any neighborhood of a point on the boundary. In essence, this means that each compact  $C^2$  manifold  $M$ , with boundary, can be considered as a submanifold of a compact  $C^2$  manifold  $N$  without boundary.

The following definition of an envelope of a surface is central to our approach. Its use was motivated by a careful examination of the proofs previously presented [9, 24, 25] for reconstructing  $C^2$  manifolds without boundary, which revealed a critical reliance upon a positive minimum dis-

tance between a surface and its medial axis. This has previously been proven for  $C^2$  surfaces [9], but the extension here required showing that there also be a positive minimum between the envelope of a  $C^2$  surface (as defined below) and the medial axis of this envelope. It is easy to show that this envelope is a surface without boundary, but, in general, the envelope will not be  $C^2$ . However, we were able to show that this envelope had sufficient smoothness to still conclude that there was a positive minimum distance between the envelope of a  $C^2$  surface and the medial axis of this envelope (The smoothness condition is stronger than  $C^1$  and is known as  $C^{1,1}$ . For more details the interested reader is referred to our theory pre-print [2] .) While optimal algorithms for computing this lower bound are still evolving, our prototype software suggests that these algorithms will have many performance and stability advantages over algorithms to approximate the medial axis. In the definition of the envelope, below, the value of  $\rho$  is less than the positive lower bound on the distance between the envelope and its medial axis. A subtle distinction about the new theory presented here is that it does *not* depend upon an *explicit* calculation of the medial axis.

**Definition 3.1** *For suitably chosen values of  $\rho > 0$ , the  $\rho$ -envelope of  $M$ , denoted  $E_\rho(M)$  is defined as*

$$E_\rho(M) = \{p \in \mathbf{R}^3 : d(p, M) = \rho\} .$$

It is *not* necessary to assume that  $M$  is orientable for our definition of the  $\rho$ -envelope, as given here. (A typical example of a non-orientable surface with boundary is a Möbius strip.) The following theorem justifies the role of the envelope and its proof is presented in related pre-prints [1, 2], which also provide the bounds on  $\rho$ .

**Theorem 3.1** *If  $M$  is  $C^2$ , then, for any  $\epsilon > 0$ , there exists a sufficiently small value of  $\rho$  such that its  $\rho$ -envelope has a minimum positive distance to its medial axis so that it is possible to explicitly define an ambient isotopic PL approximation to  $M$  via the nearest point mapping, where the distance between  $M$  and its approximation will be strictly less than  $\epsilon$ .*

### 4. Computational Examples

The details of our theory presented in our pre-print [2] show how to create approximants that are ambient isotopic to  $E_\rho(M)$ , as well as approximants that are ambient isotopic to  $M$ . The examples presented here were motivated by that theory. They were created with new code as a pre-processing interface to the Power Crust algorithm in order to produce ambient isotopic approximations to

$E_\rho(M)$ . Complete adherence to the theory of our companion paper would have also required implementation of post-processing code to extract a subset of the Power Crust output to be ambient isotopic to  $M$ . This additional code is subtle and has not yet been fully implemented. The examples presented here demonstrate a viable alternative to that full implementation. Namely, the component of the medial axis of  $E_\rho(M)$  that lies interior to  $E_\rho(M)$  is equal to  $M$ . Since the Power Crust also produces an approximation of this interior component of the medial axis of  $E_\rho(M)$ , this approximation is taken as an approximation of  $M$ . In the examples presented that compare our results with direct reconstructions from the Power Crust, again remarking, in fairness, that the Power Crust algorithm was not designed to accept surfaces with boundary.

Initial 'proof-of-concept' experiments were performed on several simple NURBS surfaces, and are presented in this paper. The techniques developed on the NURBS surfaces were then applied to a challenging set of point cloud data [15] and our improvements are discussed. This approach permitted a controlled environment to analyze the results obtain by the envelope technique. All the information necessary to produce an envelope may be found analytically in a NURBS surface representation. The normals, partial derivatives and maximum curvature can be readily obtained to produce a precise envelope. This information, together with an estimate of the minimum feature size [3], then can guide the sampling rate to guarantee an ambient isotopic approximation similar to techniques already discussed in the literature [9] which are extended in our companion theory paper [2]. The examples presented here show that an accurate envelope construction will yield a faithful and desirable reconstruction.

#### 4.1. Cylinder Example

For Figure 4, the top left is a tessellation of the quadratic NURBS cylinder. The top right presents a graphical display of an approximation of the envelope by balls centered at each vertex on the tessellation. The bottom left displays points selected along the surface normals of the cylinder at a distance equivalent to the radius of the spheres. The normals and tangents of the surface are used to define sample points on the envelope around the boundaries. The bottom right shows a point cloud set of the extent for the cylinder envelope and completes our pre-process for refining input data for the Power Crust, leading to the improved output shown in the right half of Figure 3. Similar boundary improvements are also evident in the next example.

#### 4.2. Foot Example:

The example presented here is a challenging one already seen in the literature, where one heuristic approach was created to respect the boundary [6] and an alternate method was presented to close off that boundary [15]. Here, no surface definitions were known in advance (in contrast to the other examples presented) and the point cloud data was provided by the previously cited author [15].

Figure 5 has two images. On the left is a direct reconstruction of the foot from the sample points provided using the Power Crust algorithm. This image also has an enlarged view of the boundary region near the ankle, where many artifacts are clearly visible which close the surface. The right image shows a reconstruction of the foot using the same original sample points as input to the pre-process that builds the envelope of this data. Again, there is a closer view of the boundary region near the ankle, showing that the boundary is more faithfully preserved.

Figure 6 has four images. The top left shows the original sample points for the foot, where these points were measured by a laser scan of the actual foot, and then their  $(x, y, z)$  co-ordinates were recorded in a text file. The top right shows the polar balls produced by the Power Crust, representing the radial field of the approximated medial axis of the point cloud. In this top-right image, noise is evident near the toes. The bottom left shows a sampling of poles determined from the Power Crust algorithm. The poles approximate normals to the original surface. The bottom right shows a point cloud representation for the envelope enclosure for the original point cloud. Since surface normals are central to the definition of the envelope and none are explicitly available here, envelope points are determined along the poles at a distance from the medial axis that is equivalent to the radius of the polar balls and offset in both directions. This foot envelope was constructed adaptively, where we experimented with varying the radius with location of the sample point in a modification of our definition of the envelope. This results in a tighter envelope around the toes and a slightly more generous envelope around the ankle. Along the boundary, additional points are created with user specified normals and tangents, appropriate to the envelope construction. This aspect currently remains within the judgement of the user, but the success of these experiments leads us to further investigate the theoretical constraints that would be involved formalizing this adaptive technique.

#### 4.3. Discussion of Input Needed and Final Output

Our foot reconstruction presented here significantly improves the foot boundary (near the ankle) and generally compares well with that done by heuristic methods [6]. Our advantage is a reliance upon provable techniques and a well-

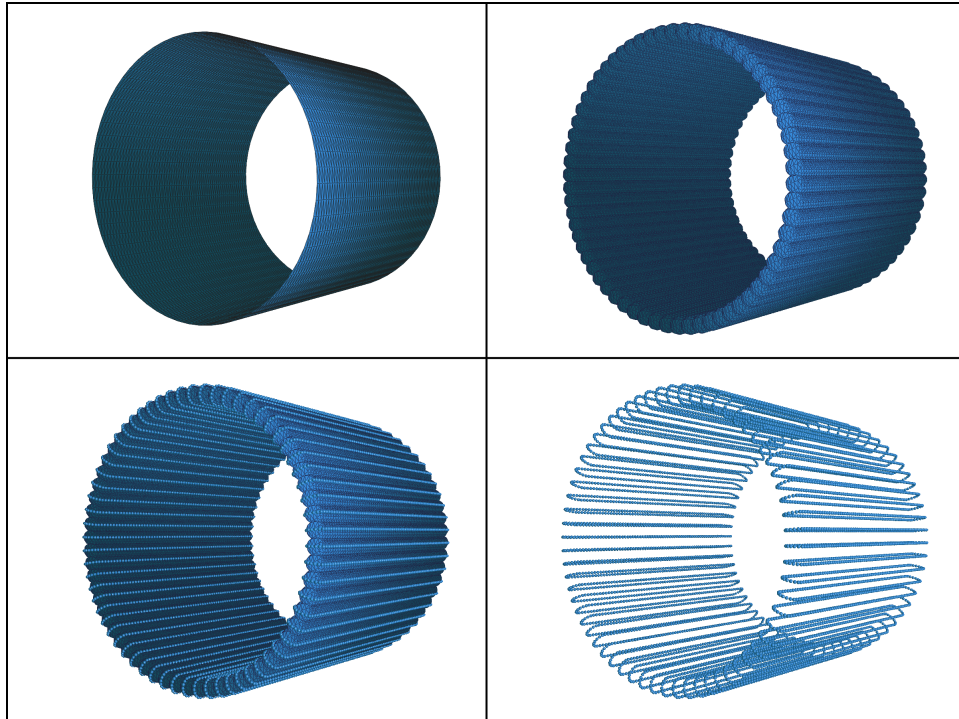


Figure 4. Cylinder

---

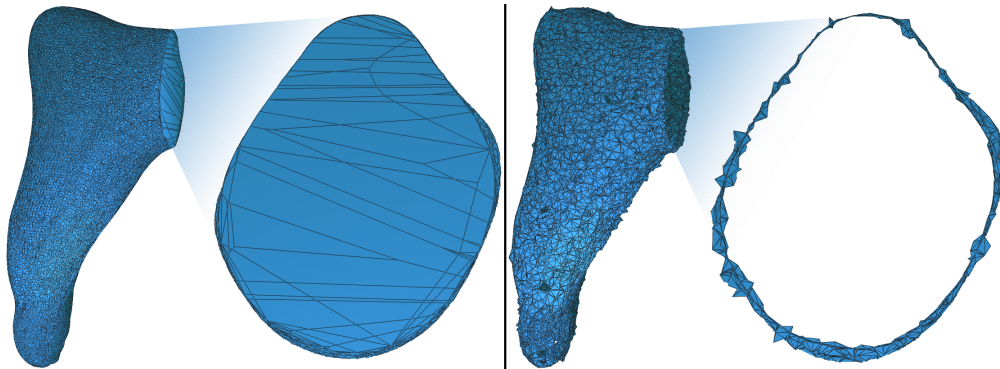


Figure 5. Comparison of Methods: Foot Data

---

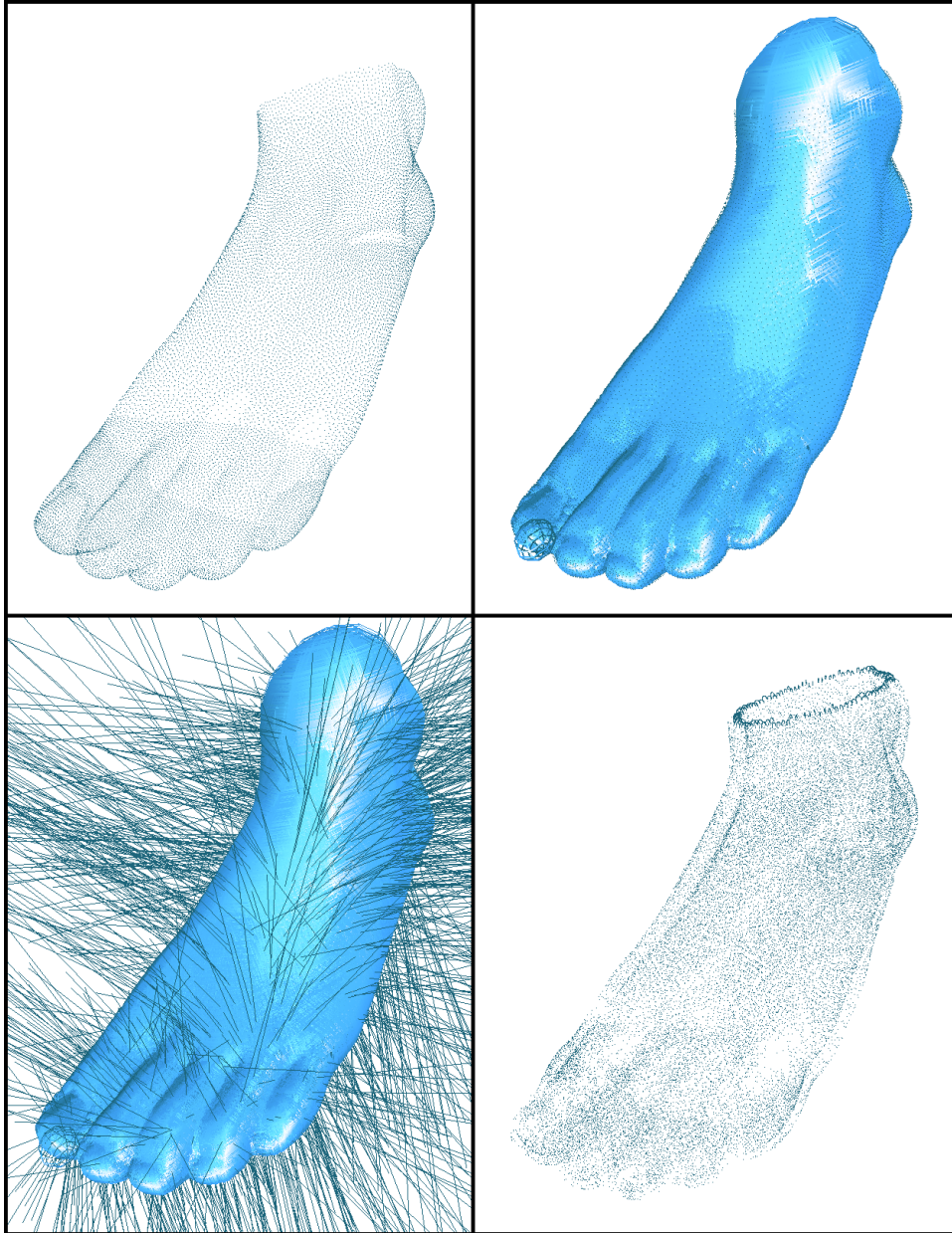


Figure 6. Stages of Method: Foot Data

defined class of permissible input surfaces. (The other primary approach to this problem [15] is not directly comparable, as it eliminated this boundary, whereas we preserve it.) However, the results of Subsection 4.2 can be compared to the other experiments to show that our reconstruction still suffers in the absence of critical geometric data, which we attribute primarily to the need to approximate normals and ball radii to use in our envelope construction technique. Those approximated normals are shown in the lower left of Figure 6 in addition to the polar balls which indicate the accuracy of the medial axis approximation. Artifacts in the foot reconstruction appear in the form of holes and local maximum/minimum that are inconsistent with the original geometry.

## 5. Discussion of Hypotheses

This section presents an example that shows our reliance upon the  $C^2$  hypothesis of Theorem 3.1. Let  $x = y^2$ , for  $y \in [0, 2]$  be rotated about the x-axis. The resulting surface of revolution is shown in Figure 7 and has a boundary at its right hand extremity.

The upper left of Figure 7 is the point cloud data sampled from equations of the paraboloid. The upper right of Figure 7 is a direct Power Crust reconstruction of previous point cloud data. Like the cylinder, this approximation of the paraboloid has no boundary, where one should exist at its right hand extremity. The lower left image displays a point cloud showing the envelope of the paraboloid. The lower right displays the reconstruction created from the envelope techniques, where, by comparison, there is a crisp boundary.

On the other hand, we note the importance of our smoothness assumptions to our implementation. For instance, consider the image shown in the left of Figure 8. It is defined as a surface of revolution of the curve  $y = x^{-(3/2)}$ . It is a surface with boundary (at the top), but it is not  $C^2$  and its resulting envelope is not  $C^{1,1}$  (which is our smoothness hypothesis for our envelopes, as described Section 3). Hence, artifacts appear near the base during reconstruction, as shown in the magnification at the right of Figure 8. The underlying algorithmic causes remain the subject of further investigation.

## 6. Accurate Normals and Sampling Density

This section shows typical data of experiments done to better understand the roles of accurate normals and sampling density.

### 6.1. Approximating Normals

Figure 9 shows how the resultant surface approximation varies with the accuracy of the approximation. The progression from left to right is of decreasingly accurate normals. The suggestion to investigate this relationship further arose from our previously discussed reconstruction with the foot data. There, improving the normals along the boundary resulted in significant improvements to the final surface approximation.

### 6.2. Sampling Density of Knots

The knot surface reconstructions of this subsection are, also, all of surfaces with boundary. The intent is to create surfaces based upon the unknot and the trefoil knot. Those original surfaces were created by drawing each knot as a curve and then these curves were extended into surfaces by a linear extrusion which produced no self-intersections. Each surface is like a ribbon with the corresponding knot for its two boundary curves.

To indicate the type of difficulties that can occur in approximating these unknot surfaces, we first show an example of the difficulties that can occur in merely approximating the unknot curve, as previously reported [9]. On the left of Figure 10 is shown a particular example of the unknot curve, which is not planar. The resulting piecewise linear approximation on the right is no longer the unknot, but has four essential crossings, as a result of picking sampling points that are so far apart that the approximation no longer has the same knot type or embedding as the original curve. This should serve to motivate the following study of the relation between sampling density and topological characteristics in reconstruction of an unknot surface.

Figure 11 shows the expected pattern of the reconstruction improving with higher sampling density, depicted for the unknot. In this unknot surface example, its envelope surface was then constructed at varying radii,  $\lambda$ , decreasing from right to left, while the sampling density of points from each envelope was kept constant. On the extreme right of the series of images, denote the radius of this envelope as  $\lambda_6$ . The value of  $\lambda_6$  is sufficiently large that there is a perceptible artifact towards the center of this image, where there appears to be a self-intersection or an undercrossing in  $\mathbf{R}^3$  (as did appear in Figure 10), although none should occur. Likely, this was caused by having the value of  $\lambda_6$  exceed the value for  $\rho$ , as given in Theorem 3.1, but more precise numerical studies are needed to verify this condition. For comparison, if one views the images in middle of this sequence, the smaller values of  $\lambda$  yield better images of the unknot. Proceeding to the left-most image, its radius of  $\lambda_1$  is so small that the least feature size criterion of the Power Crust algorithm would require a much finer sampling den-

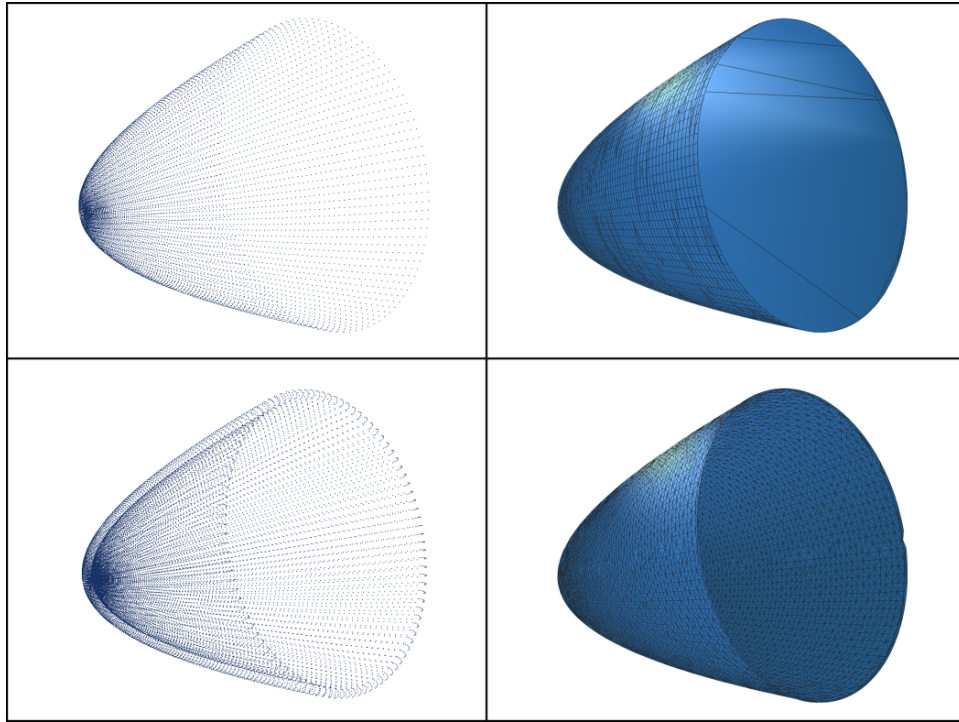


Figure 7. The reconstruction of a paraboloid

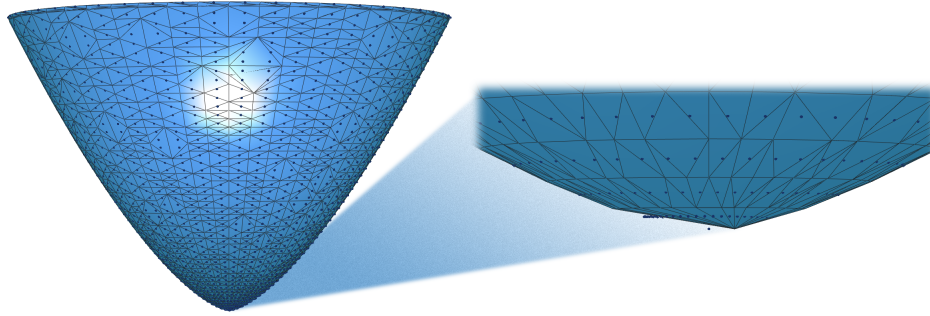
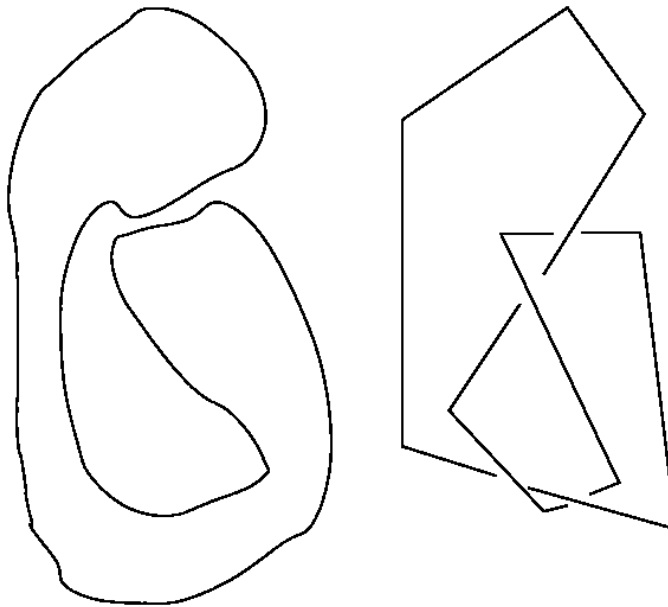


Figure 8. Not  $C^{1,1}$



Figure 9. Noise in Normals

---



**Figure 10. Bad Approximation of Unknot**

---

sity of the envelope than the constant density that is being maintained. Since the sampling density is no longer sufficient, holes and other visual artifacts begin to appear in the resulting reconstruction. Hence, this study shows the balance required between sampling density and radius chosen for the envelope surface.

This unknot study then led to consider the more challenging trefoil knot surface, as a comparison of our envelope reconstruction method versus techniques that have already appeared in the literature. That visual comparison has already been presented in Figures 1 and 2.

## 7. Concluding Remarks and Future Work

An improved surface reconstruction technique is demonstrated for  $C^2$  manifolds with boundary, where the method is dependant upon definition and implementation of an auxiliary surface, called the envelope. The promising results achieved here were by an effective expedient. We used the component of the medial axis of an envelope surface that is contained in the interior of the envelope as an approximation to the original manifold. An approximation to this component is already produced by the Power Crust algorithm and the results presented here show this to be a good approximation in practice.

It can be shown that a compact  $C^2$  manifold  $M$ , with boundary, is equal to the interior component of the medial axis of the  $\rho$ -envelope of  $M$ , denoted as  $E_\rho(M)$ , for suitably chosen values of  $\rho$ . Hence, in principle, the expedient used here is well-founded, but there remain some issues for further investigation. Namely, the Power Crust nec-

essarily produces an approximation of the medial axis, so, if there are any deviations of this approximation from the true medial axis, then no formal topological guarantees can be given for the examples presented here. This remains the subject of further investigation, but the results presented here are promising that more detailed investigation will be fruitful.

The experiments conducted provide interesting information about the role of accurate normal approximations in reconstructing surfaces with boundary. Furthermore, the images produced of other numerical experiments help to visualize the interplay between topological embedding of the original manifold and required sampling density. Further work needs to be done on both these subjects, towards optimal sampling criteria, which is a subject of broad ongoing interest.

## 8. Acknowledgements

The following funding sources are acknowledged, with appreciation. Partial funding for K. Abe was from NSF grants CCF 0429477 and CCR 0226504. Partial funding for J. Bisceglia and D. R. Ferguson was from NSF grant DMS-0138098. Partial funding for T.J. Peters was from NSF grants CCF 0429477, DMS 0138098 and CCR 0226504. Partial funding for A.C. Russell was from NSF grants CCF 0429477 and CCR 0226504. Partial funding for T. Sakkalis was obtained from NSF grants DMS-0138098, CCR 0231511, CCR 0226504 and from the Kawasaki chair endowment at MIT. All state-

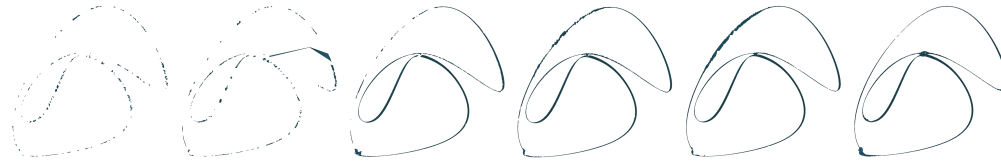


Figure 11. Unknot

ments in this publication are the responsibility of the authors, *not* of these funding sources.

## References

- [1] K. Abe et al. Computational topology for reconstruction of surfaces with boundary, part i: Applications. *Pre-print*, [www.cse.uconn.edu/~tpeters](http://www.cse.uconn.edu/~tpeters), pages 1–23, 2004.
- [2] K. Abe et al. Computational topology for reconstruction of surfaces with boundary, part ii: Mathematical foundations. *Pre-print*, [www.cse.uconn.edu/~tpeters](http://www.cse.uconn.edu/~tpeters), pages 1–15, 2004.
- [3] N. Amenta and M. Bern. Surface reconstruction by voronoi filtering. *Discrete and Computational Geometry*, 22:481–504, 1999.
- [4] N. Amenta, M. Bern, and M. Kamvysselis. A new voronoi-based surface reconstruction algorithm. In *Proc. ACM SIGGRAPH*, pages 415 – 421. ACM, 1998.
- [5] N. Amenta, S. Choi, T. Dey, and N. Leekha. A simple algorithm for homeomorphic surface reconstruction. In *ACM Symposium on Computational Geometry*, pages 213–222, 2000.
- [6] N. Amenta, S. Choi, and R. Kolluri. The power crust. In *Sixth ACM Symposium on Solid Modeling*, pages 249–260. ACM, June 2001.
- [7] N. Amenta, S. Choi, and R. Kolluri. The power crust, union of balls and the medial axis transform. *Computational Geometry: Theory and Applications*, 19:127–173, 2001.
- [8] N. Amenta et al. Emerging challenges in computational topology. In *Workshop Report on Computational Topology*. NSF, June 1999.
- [9] N. Amenta, T. J. Peters, and A. C. Russell. Computational topology: ambient isotopic approximation of 2-manifolds. *Theoretical Computer Science*, 305:3–15, 2003.
- [10] L.-E. Andersson, T. J. Peters, and N. F. Stewart. Equivalence of topological form for curvilinear geometric objects. *International Journal of Computational Geometry and Applications*, 10(6):609–622, 2000.
- [11] J.-D. Boissonnat and S. Oudot. Provably good surface sampling and approximation. In *Eurographics Symposium on Geometry Processing*, pages 9–18, 2003.
- [12] W. M. Boothby. *An introduction to Differentiable Manifolds and Riemannian Geometry-Second Edition*. Academic Press, New York, 1986.
- [13] T. Culver, J. Keyser, and D. Manocha. Accurate computation of the medial axis of a polyhedron. In *Proceedings of Fifth Symposium on Solid Modeling and Applications*, pages 179–190. ACM, June 1999.
- [14] T. K. Dey, H. Edelsbrunner, and S. Guha. Computational topology. In *Advances in Discrete and Computational Geometry (Contemporary Mathematics 223)*, pages 109–143. American Mathematical Society, 1999.
- [15] T. K. Dey and S. Goswami. Tight cocone: a water-tight surface reconstructor. In *Eighth ACM Symposium on Solid Modeling and Applications*, pages 127–134. ACM, June 2003.
- [16] T. K. Dey, H. Woo, and W. Zhao. Approximate medial axis for cad models. In *Eighth ACM Symposium on Solid Modeling and Applications*, pages 280–285. ACM, June 2003.
- [17] A. Gain and A. Dodgson. Preventing self-intersection under free-form deformation. *IEEE Trans. on Visualization and Computer Graphics*, 7(4):289–298, 2001.
- [18] M. Gopi. On sampling and reconstructing surfaces with boundaries. *Yes*, 13(1):43–72, 2002.
- [19] M. W. Hirsch. *Differential Topology*. Springer-Verlag, New York, 1976.
- [20] W. Macy. Personal communication. 2003.
- [21] T. Maekawa, N. M. Patrikalakis, T. Sakkalis, and G. Yu. Analysis and applications of pipe surfaces. *Computer Aided Geometric Design*, 15(5):437–458, 1998.
- [22] M. Mäntylä. Computational topology: A study on topological manipulations and interrogations in computer graphics and geometric modeling. *Acta Polytechnica Scandinavica, Mathematics and Computer Science Series*. Finnish Academy of Technical Sciences, Helsinki, 37, 1983.
- [23] H. Pottmann and M. Peternell. Envelopes computational theory and applications. In *Spring Conference on Computer Graphics 2000*, pages 3–23. Comenius University, Bratislava, May 2000.
- [24] T. Sakkalis and T. J. Peters. Ambient isotopic approximations for surface reconstruction and interval solids. In *Eighth ACM Symposium on Solid Modeling and Applications*, pages 176–184. ACM, June 2003.
- [25] T. Sakkalis, T. J. Peters, and J. Bisceglia. Isotopic approximations and interval solids. *CAD*, 36 (11):1089–1100, 2004.
- [26] S. Willard. *General Topology*. Addison-Wesley Publishing Company, Reading, MA, 1970.